Robotica (2014) volume 32, pp. 97–114. © Cambridge University Press 2013
doi:10.1017/S0263574713000659

UAV-borne X-band radar for collision avoidance

Allistair Moses†, Matthew J. Rutherford‡*, Michail Kontitsis† and Kimon P. Valavanis†

†*Department of Electrical and Computer Engineering, University of Denver, Denver, CO, USA*
‡*Department of Computer Science, University of Denver, Denver, CO, USA*

(Accepted June 7, 2013. First published online: July 19, 2013)

SUMMARY
The increased use of unmanned aerial vehicles (UAVs) is coincidentally accompanied by a notable lack of sensors suitable for enabling further improvement in levels of autonomy and, consequently, integration into the National Airspace System (NAS). The majority of available sensors suitable for UAV integration into the NAS are based on infrared detectors, focal plane arrays, optical and ultrasonic rangefinders, etc. These sensors are generally not able to detect or identify other UAV-sized targets and, when detection is possible, considerable computational power is typically required for successful identification. Furthermore, the performance of visual-range optical sensor systems may suffer when operating under conditions that are typically encountered during search and rescue, surveillance, combat, and most other common UAV applications. However, the addition of a miniature RADAR sensor can, in consort with other sensors, provide comprehensive target detection and identification capabilities for UAVs. This trend is observed in manned aviation where RADAR sensors are the primary on-board detection and identification sensors. In this paper, a miniature, lightweight X-band RADAR sensor for use on a miniature (710-mm rotor diameter) rotorcraft is described. We present an analysis of the performance of the RADAR sensor in a realistic scenario with two UAVs. Additionally, an analysis of UAV navigation and collision avoidance behaviors is performed to determine the effect of integrating RADAR sensors into UAVs. Further study is also performed to demonstrate the scalability of the RADAR for use with larger UAV classes.

KEYWORDS: Sensor or actuator design; Aerial robotics; Mechatronic systems; Mobile robots; Navigation.

1. Introduction

The quantity and capability of inexpensive, off-the-shelf, component-based unmanned aircraft has steadily increased in recent years. This has had a profound impact on the development of unmanned aircraft systems lighter than 25 kg. Unmanned aircraft based on inexpensive platforms are now readily available and are utilized in numerous commercial applications such as surveillance, traffic monitoring, search and rescue, building inspection and accident investigation, to name just a few. While the availability of these platforms is beneficial in general, it does highlight several potential challenges of their widespread use for non-military applications. First, as there is currently no training nor certification process for unmanned aerial vehicle (UAV) pilots, the vehicles are operated by users who often lack the necessary experience to safely fly these vehicles in close proximity to other unmanned systems or, more importantly, manned air traffic. On the other hand, the number of fully autonomous (regardless of the exact definition of this term) unmanned systems is increasing, and this trend is likely to continue for the foreseeable future. These fully autonomous vehicles generally sense their position by means of satellite navigation systems (e.g. GPS, Galileo, GLONASS, and COMPASS), and transmit data (for example, in the form of video) to their operator. Additional information about the environment is obtained using ultrasonic or laser rangefinders, pressure sensors, or a plethora of application-specific sensors that may be mounted on the vehicle. Beyond these

* Corresponding author. E-mail: matt.j.rutherford@gmail.com

sensors and other payload (if any), many unmanned systems are virtually "blind" with respect to their environment, and not under the guidance of ground-based air traffic control. Consequently, these vehicles are prone to become involved in mid-air collisions involving manned aviation.

We believe this situation can be mitigated by the use of miniature radio detection and ranging (RADAR) sensors on unmanned vehicles. This is based on the idea that RADAR sensors are capable of representing target data in a fashion that is not easily replicated by other sensors. For example, cameras and other optical sensors require significant computational power to practically perform detection and identifications functions in real time, while being incapable of functioning correctly in adverse conditions. Although such sensors do exist in relatively small form factors (e.g. the latest generation of heat-seeking air intercept missiles, AIM-9x etc), these sensors are not designed for deployment on miniature vehicles as their weight and active cooling requirements would significantly reduce the operational flight time of these small vehicles. Additionally, the proliferation of battery or fuel cell-powered electrically propelled vehicles makes detection by thermal signatures difficult due to the comparatively low operating temperatures within the vehicle.

RADAR sensors, on the other hand, provide a number of advantages over optical see-and-avoid systems:

1. If a continuous wave Doppler illumination scheme is used, the return signal is generally composed of both moving targets and the motion of the vehicle carrying the RADAR illuminator (relative to the environment). Since most autonomous vehicles are equipped with an inertial measurement unit, attitude reference system, positioning system, or other form of motion measuring equipment, the vehicle's motion can be subtracted from the Doppler returns, thus ideally leaving only the target vehicle signatures.
2. The longer wavelength allows for the illumination and detection of unique vehicle features typically not observable with optical sensors. For example, jet engine compressor blades are not likely to be useful when using an optical sensor, but a RADAR sensor can differentiate between compressor blade characteristics relatively easily.
3. RADAR sensors allow for increased flexibility with regard to their installation on the host vehicle. Indeed, the antennas can be made structural components of the UAV or blended into the skin of the vehicle.

The purpose of this paper is to describe the development of a miniature RADAR system, and the algorithms that enable this RADAR system to detect, identify, and subsequently evade air traffic. The approach is general and the prototype RADAR system may be scaled up to be suitable for larger UAVs. The work presented herein is a compilation our two previous papers.[1,2] The novelty and primary contribution of these papers is the use of the Doppler shift induced by the UAV's propulsion system. This identification information can then be used to improve the collision avoidance maneuvers used by the host UAVs. While this theory can be applied to larger, manned vehicles, refs. [1, 2] apply this theory to a miniaturized sensor suitable for use on and against miniature UAVs.

The remainder of this paper is organized as follows. Section 2 provides background information on the basic principles of the operation of the RADAR. Section 3 describes alternate approaches to collision avoidance in aerial vehicles. Section 4 describes the prototype RADAR system in detail, and Section 5 presents the data processing algorithms along with some results from the initial testing phase. Section 6 presents further evaluation of the RADAR system including outdoor experiments. Section 7 outlines an analysis of the proposed RADAR system used in the NAS. Section 8 concludes the paper.

2. Background Information

RADAR utilizes electromagnetic energy (typically in the microwave range) to gather information on remote objects by analyzing the characteristics of their reflected energy. Most large-scale RADAR installations utilize some form of pulsed RADAR arrangement to extract information related to the targets by timing the RADAR returns. However, the complexity, limited range resolution, and large minimum range of pulsed RADAR sensors preclude their adoption for miniature UAV applications. These issues are resolved through the use of continuous wave (CW) RADARs.

CW RADAR sensors can be divided into two generalized forms: frequency-modulated continuous wave (FMCW) RADAR and Doppler RADAR. The former utilizes periodic variations in frequency to

determine the range to the target. The latter relies on the Doppler effect to isolate moving targets and determine their velocities relative to the RADAR antenna, but it is incapable of determining the range to the target. The hardware described in this paper is capable of both FMCW and Doppler operations. However, only the Doppler operation mode is utilized in the current prototype. A practical sensor might operate in the Doppler mode until a target is detected, and then the FMCW mode to provide range data to the target. In this fashion, the false alarm rate can be kept low by only responding to targets with some radial velocity relative to the RADAR. Furthermore, the overall reaction time is decreased by the use of the Doppler mode since a target's presence and velocity can be acquired from a single sample window, whereas FMCW must use multiple sample windows to determine the velocity based on the differentiated ranges.

At the heart of the Doppler RADAR operation is the Doppler frequency shift generated by some combination of moving sources and/or targets. For co-located transmit and receive antennas, Eq. (1) defines the Doppler shift as a function of the target velocity relative to the transmit antenna v, the transmitted frequency F_t, and the speed of light c. An analysis of Eq. (1) reveals that for low velocity targets, Eq. (1) can be simplified into Eq. (2) given $F_t = 10.5$ GHz (selected due to a compromise between the component acquisition costs and the size of the target). Utilizing this information, we can determine the velocity of various targets by measuring the frequency shift:

$$\Delta F = F_t \left(\frac{2v}{C - v} \right), \tag{1}$$

$$\Delta F = 70.048v. \tag{2}$$

For advanced UAV-based control applications, it is necessary to both determine target velocity and identify the target in question. As most air vehicles, while in operation, consist primarily of rotating components moving in a periodic manner, there exists a unique Doppler signature for most vehicles. *A priori* knowledge of this signature can be utilized in real time to determine the presence of a familiar target vehicle within the currently imaged scene. For example, the Align TRex-450Pro helicopter Doppler signature can be expressed as having frequency peaks described by Eq. (3):

$$S_{\text{Heli}} = \left(\frac{2F_t\pi}{CT} \right) \left[d_{mr} + d_p + \frac{d_{tr}}{1/4.24} \right] + \text{Aux}(T), \tag{3}$$

where d_{mr}, d_p, and d_{tr} are the diameters of the main rotor, paddles, and tail rotor, respectively. Note that the scaling factor 4.24 applied to the tail rotor frequency component is due to the gear ratio between the main and tail rotors. F_t is the transmit frequency, c is the speed of light, and T is the rotational period of the rotor system. Aux(T) represents additional components within the helicopter (e.g. the motor, main and tail rotor transmissions, and drive shafts). While these components do contribute to the overall Doppler signature, they are neglected due to their relatively small size and the difficulty in producing a model incorporating all these components. Essentially, the model is a representation of the velocities caused by the moving vehicle components. As each vehicle class is described by a different model, the quantity and location of frequency peaks act as a "fingerprint" for vehicles of the class. Although Eq. (3) assumes that the velocity of a rotating part is concentrated at a single point, when in practice it is distributed over the length of the part, the actual signatures observed in practice are different enough that identification is still possible (as depicted in Fig. 7).

3. Related Work

Active RADAR sensors are not the only solution for airborne collision avoidance. There exist a number of both active and passive collision avoidance systems (e.g. TCAS, PCAS, and FLARM) that aim to address this issue in virtually all sectors of manned aviation.[3] The traffic collision avoidance system (TCAS) consists of a radio frequency (RF) transponder located on all TCAS-equipped aircraft. This transponder is coupled with a cockpit display and the appropriate antenna arrangement. TCAS functions by communicating with all the transponders of other TCAS-equipped aircraft within the area and estimating the three-dimensional motion vector of the detected TCAS units. If the TCAS transponder detects the possibility of a collision, the pilot is notified via cockpit displays. The TCAS

system may instruct the pilot to make an altitude change to avoid the collision or perform other maneuvers. TCAS is generally required on all aircraft exceeding 5700 kg or carrying more than 19 passengers.[4] The TCAS equipment also exists in a passive version, namely the portable collision avoidance system (PCAS). Essentially, PCAS is a TCAS system without the transmit electronics. Instead, the PCAS receiver passively receives data from other local TCAS modules, and then directs the pilot to avoid a collision course. Generally, TCAS modules are significantly more expensive than PCAS modules, with costs for full TCAS systems often exceeding 50,000 USD.[5] This is contrasted with a simple PCAS receiver which can be obtained for 550 USD.[6] However, while any PCAS-equipped vehicle can see all other TCAS-equipped vehicles, they cannot be seen, and two PCAS-equipped vehicles will be blind to each other, so the cost savings clearly come with severely diminished capability.

Another solution is FLARM (derived from "flight alarm") that is popular with glider pilots, and operators of low flying vehicles. It serves to address the same scenario targeted by the TCAS. The primary difference between the two is the proximity with which slow, low flying aircraft can safely co-exist. The use of TCAS in these situations would often result in an undesirable rate of false-positive collision warnings. FLARM is similar to TCAS in that data are communicated from aircraft to aircraft without the need for ground-based coordination. However, FLARM further reduces acquisition costs by utilizing satellite navigation technology to determine the flight paths. This information is then broadcast to other FLARM devices within range.[7] FLARM, however, has certain disadvantages. For example, FLARM devices are used in several European countries but have yet to be used in the Americas due to various wireless communication regulatory committees.[8]

In summary, all current, commercially available, airborne collision avoidance systems utilize cooperative information sharing between on-board transponder units to detect collision courses between aircraft and subsequently display a warning to the pilot. However, these commercially available collision avoidance systems are incapable of detecting a collision when only one vehicle in the colliding pair is equipped with a suitable transponder. Therefore, one can expect that to further increase safety, every vehicle in the airspace must be equipped with identical collision avoidance systems. As this situation is unlikely to occur, there exists a need for a collision avoidance system that can function independently of a homogeneous, transponder-based, cooperative environment. Additionally, transponder-based systems such as TCAS and FLARM assume that all vehicles are essentially on equal footing and they are activated only in emergency situations (i.e., when flight path planning from ground-based air traffic controllers has somehow gone wrong), and both vehicles on a collision course are simply trying to avert disaster. In the future NAS, unmanned vehicles will not (typically) be under control of ground-based air traffic controllers; they will be expected to impact regular manned air traffic as little as possible, so unmanned aviation in general must be able to successfully navigate around manned vehicles intelligently. This need is the primary motivation behind the design of the prototype RADAR system. As a first step, the system is evaluated using miniature aerial vehicles. This is justified by the need to eliminate as many Doppler sources as possible (e.g. cars, pedestrians, and wind-blown trees), while simultaneously reducing the risk to the test operators and the vehicles themselves.

4. Prototype RADAR Description

From inception through all phases of development, every component of the prototype RADAR system has been designed such that it could be deployed on a wide variety of aerial vehicles. Due to this requirement, a modular approach has been selected to allow the individual sensor components of the RADAR system to be dispersed over the vehicle structure, thus simplifying the vehicle mass distribution requirements. Indeed, virtually any UAV capable of supporting a payload as described in Table I can be equipped with this RADAR system. Furthermore, a variety of different module combinations can be selected to suit a range of applications and scenarios. This enables an optimized sensing solution to be rapidly developed for most UAV systems. For example, if a different transmit frequency is desired, only the RF component of the prototype RADAR sensor must be changed. Likewise, if the current antenna arrangement is not suited for a particular application, another antenna can be used since the RF component utilizes industry standard waveguide components. The prototype RADAR sensor is shown in Fig. 2.

Table I. Sensor specifications.

Sensor mass	230 g
Sensor dimensions	15.5, 10, 9 cm
Power consumption	4.5 W
Input voltage range	10–42 VDC
Transmit frequency	10.5 GHz
Transmit power	10 mW
Range (against 1-m^2 RCS target)	66 m

4.1. Hardware configuration

The first module of the prototype RADAR system to be described is the RF front-end module. The design of this component is critical for the correct function of the overall RADAR system. Therefore, all efforts were focused on utilizing efficient technologies with a proven track record. The specific function of this module is to generate, transmit, receive, and finally, downconvert the received signal to be used in subsequent stages. Several architectures were investigated for this task. The first design iterations utilized PCB-mounted discrete components. However, these designs suffered from significant losses due to the high frequencies involved and the losses incurred when coupling the front end to the antenna. These problems were eventually solved by utilizing a relatively common waveguide-based microwave device known as a Gunnplexer. The Gunnplexer consists of a Gunn diode mounted within a resonant cavity. Also located within the cavity are a ferromagnetic circulator and a mixing diode. The Gunn diode functions as a voltage-controlled microwave source. The microwave energy from the oscillator is then divided between the mixing diode and the antenna. The portion of the energy diverted in the mixing diode functions as the local oscillator signal, which is mixed with the energy reflected from the target. This mixing process (frequency domain multiplication) produces an output known as the intermediate frequency (defined as $\delta(F_L - F_R)$), where F_L is the local oscillator frequency, F_t is the transmit frequency, F_R is the frequency of the received radiation, and n is used to signify the nth harmonics. Additionally, other undesirable frequencies are produced, which are filtered at a later stage. The output is given in terms of

$$\text{Output} = \delta(F_L - F_R) + \delta(F_L + F_R) + \delta(nF_R) + \delta(nF_L) + \delta(nF_t). \tag{4}$$

The signals to and from the Gunnplexer are conveyed to and from the environment by means of an antenna whose primary function is to shape the electromagnetic radiation transmitted from the Gunnplexer, and to increase the range of the sensor by presenting a larger aperture to the return signals. During development, numerous antenna designs were evaluated including helical, phased array patch, and parabolic. Evaluation, using software packages such as Antenna Magus, determined that a horn antenna is the simplest solution that would provide adequate gain given the following constraints:

- *Low mass*. As the sensor is destined for UAV applications, overall sensor mass is a critical consideration. Horn antennas may be fabricated from nearly any material, provided a conductive coating thicker than the skin depth is deposited on the interior.[9]
- *Simple internal structure*. Horn antenna designs can be fabricated from simple materials without depending on specific internal periodic structures as opposed to slotted waveguide arrays or phased array patch antennas.
- *High gain and directivity*. Horn antennas provide excellent gain characteristics, given their complexity.
- *Low loss*. Direct coupling with the Gunnplexer assembly dramatically lowers insertion loss and thereby improves performance. Other designs typically require a waveguide to coaxial adapter in addition to other impedance-matching structures within the antenna.

While the primary motivating force behind the antenna design is the performance of the RADAR system, the application environment is also of great importance. As this is a RADAR system currently designed for miniature UAV applications, the antenna, and the resulting radiation pattern, must be compatible with the carrying vehicle. For rotorcraft-based airborne target detection, identification, and avoidance applications, a forward-looking field of view is desired. This requirement places a

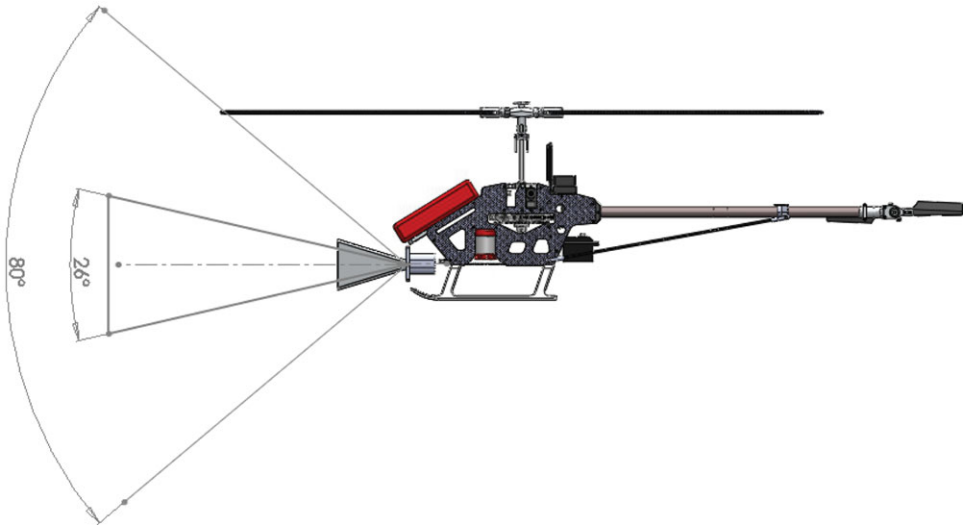

Fig. 1. (Colour online) Interaction between the main lobe and the carrying vehicle.

restriction on the maximum main lobe angle, otherwise undesired noise will be introduced into the system as a result of an interaction between the antenna main lobe and the host vehicle propulsion system. Although some level of interaction is inevitable, every effort must be made to reduce this. Figure 1 demonstrates this situation for miniature helicopter UAVs. The main lobe angle of the antenna discussed here is approximately 26° while the gain of the antenna is >17 dBi. To provide threat azimuth information, the antenna assembly is mechanically scanned such that the antenna boresight is swept through the desired field of view.

After undergoing the frequency domain multiplication as previously described, inbound signals pass through the intermediate frequency amplifier (IF amp) module. The primary function of this module is to amplify the relatively weak signal resulting from the frequency downconversion performed within the RF front end. Its secondary function is to filter the IF signal before and after each gain stage. This processing occurs in two stages. The first stage serves to present the mixing diode with a high impedance load and to attenuate undesirable signal characteristics. The first of these is the input signal DC bias. This is caused both by imperfect isolation parameters within the Gunnplexer circulator and targets with no radial velocity. Both factors result in identical F_R and F_L frequencies which, after downconversion, give rise to a DC voltage. The second unwanted signal is the high frequency (F_R+F_L) sum frequency. Following the removal of these components, the signal voltage is amplified by the first gain stage (gain $= 11\frac{V_{\text{out}}}{V_{\text{in}}}$). Subsequent to the first gain stage, the signal is sent through a high-pass filter to remove the DC offset generated by the first gain stage and remove low-frequency interference (e.g., 60/50 Hz mains frequencies and motor speed controllers) present within the signal. Finally, the signal is sent through the second gain stage (gain $= 6267\frac{V_{\text{out}}}{V_{\text{in}}}$) and is ready for digitization. The total voltage gain of the IF amplifier module is $68{,}937\frac{V_{\text{out}}}{V_{\text{in}}}$. This staged amplification process is essential for proper sensor operation. If amplification is performed in a single stage, the noise present within the intermediate frequency would saturate the amplifier output.

In order to further reduce the influence of noise on the sensor, the amplifier module is mounted directly on the Gunnplexer body. This reduces the length of the conductor that carries the low voltage signal from the mixing diode. The complete analog section of the RADAR system, when combined to the RF module, results in a mass of 137 g.

Once the signal has been received and amplified by the analog modules, it is digitized. This is performed by a 16-bit, 250 ksps, analog digital converter (ADC).[10] The Shannon–Nyquist theorem states that to accurately measure a signal without aliasing, one must sample the signal at twice the maximum frequency present within the signal. In this case, we are sampling the IF signal, so by the application of Eqs. (1) and (2), we learn that given the sampling frequency of 250 ksps the maximum measurable frequency is 125 ksps, which corresponds to a maximum measurable target velocity of

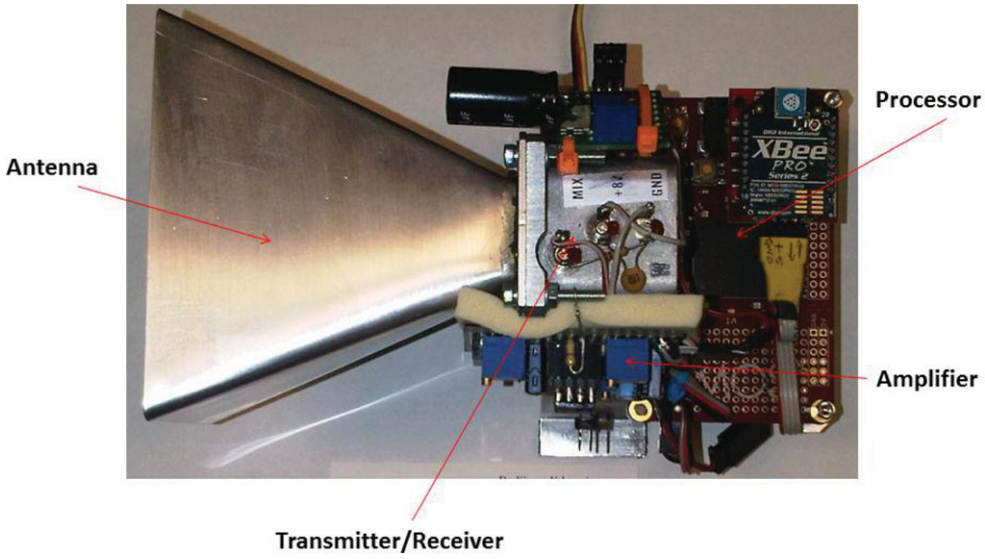

Fig. 2. (Colour online) Complete RADAR system.

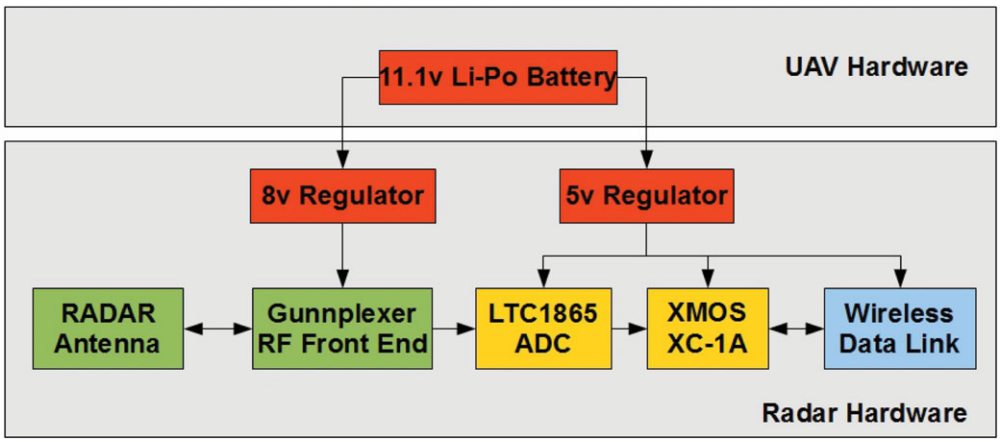

Fig. 3. (Colour online) RADAR system hardware diagram.

1784 m/s. In practice, for most UAV applications, the need to track objects with this velocity will most likely never arise due to the relatively low cruising speeds of most UAVs. Thus, the ADC sampling rate is varied to form a compromise between target velocity ranges, velocity resolution, and, finally, sensor memory limits. The varying sampling rate is achieved by introducing a delay after each ADC sample. Upon sampling, all on-board processing is performed on a 1600-MIPS, four-core, multi-threaded microprocessor (XMOS XS1-G4). The parallel processing enabled by this hardware is essential to achieving high performance levels in that it enables the pipelining of data operations. Given the computation power of this microprocessor and the simple algorithms used, the sensor detection speed is limited by the need to decrease the sampling frequency to increase the frequency resolution, not by computational complexity.

The complete prototype RADAR system, see Figs. 2 and 3, consists of the RF component, analog amplifier, signal processing boards, wireless telemetry, and mounting brackets, and hardware. The overall RADAR system specifications are displayed in Table I. Figure 4 displays the RADAR system mounted on a low-cost, commercially available quadrotor, the Parrot AR drone.

4.2. Software

The on-board processing software is composed of several discrete modules, as shown in Fig. 5. The architecture of the XMOS processor allows for software to be cleanly organized as different tasks with high-performance channels between them. In Fig. 5, the first two (green) rectangles represent the

Fig. 4. (Colour online) MAV equipped with the RADAR system.

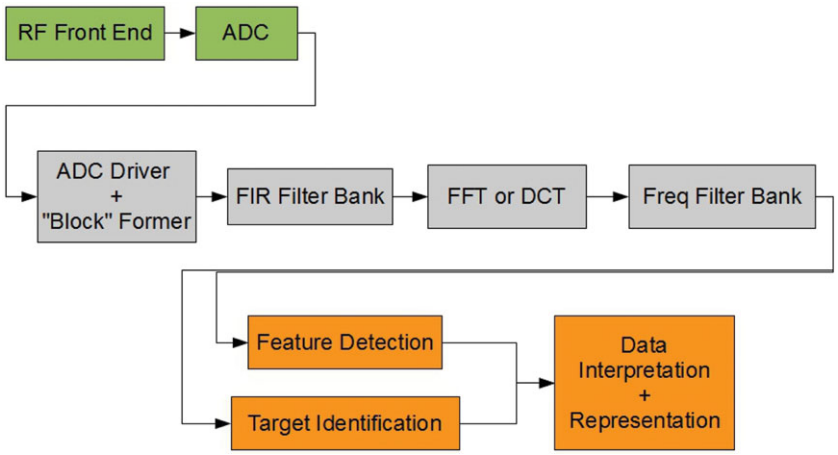

Fig. 5. (Colour online) Data pipeline overview.

hardware modules described above. The rectangles in the second row are implemented on the XMOS processor as tasks, with the arrows between them representing unidirectional data channels. The use of channels for inter-task communication obviates the need for sophisticated (and error prone) synchronization to protect shared global memory, and allows each task to perform blocking I/O on the ports/channels it is concerned with, again resulting in clean, maintainable software. Each module is executed, in parallel, as a distinct task. The hardware-based scheduler on the XMOS ensures that all tasks are scheduled fairly and with great regularity (round-robin among the active tasks for a single instruction). The "ADC driver" module samples the ADC continuously and generates data packets that are forwarded to the other modules. This essentially takes discrete measurements of the intermediate frequency amplitude and stores them in memory. The size of the data packets is variable as a function of the desired frequency resolution and velocity range—for this prototype a fixed size of 512 samples is used (the 512 bin fast Fourier transform, FFT, was selected as a compromise between target velocity resolution and on-board memory constraints). The second module consists of a set of finite impulse response (FIR) filters. These filters serve to eliminate variable noise that was not attenuated by the IF amplifier module. This approach is particularly effective as digital filters can provide steep roll-off rates, and can be implemented within the microcontroller as dictated by application requirements. For example, if the UAV is operating near power lines, a 60-Hz FIR notch filter can be introduced to enable successful operation without interference from the power lines.

The third module consists of a FFT operation required to generate frequency domain information. The fourth module is an additional digital filter block used to filter the frequency domain signal representation. This filtering is used to eliminate erroneous target information and increases the reliability and simplicity of subsequent processing blocks.

The output of the first four software modules depicted in Fig. 5 is a 256-bin frequency-domain signature (we discard the "bottom" 256 bin from the FFT as they are simply a mirror of the ones we use). This signature is now ready for use in target detection and identification.

5. Target Data Processing

As depicted in Fig. 5, target data processing can be divided into two generalized scenarios: point target detection and complex target identification. In the first scenario, the targets consist of a single object with either no or ignored internal structure. That is to say, the entire target object and all components can be considered to be traveling at the same velocity. In this mode, identification is not possible, but target velocity is readily available.

Multiple targets can be detected and their velocities, relative to the boresight vector (i.e. the vector indicating the direction of the main lobe), can be determined. However, this functionality is limited by the velocity differences between the individual targets and the Doppler-generated bandwidth occupied by the targets.

The second scenario is characterized by a target of suitable complexity (i.e. a vehicle) within the prototype RADAR main lobe. In this situation, a complex target is defined as having numerous periodically moving parts which is required for reliable sensor operation.

5.1. Simple "point" targets

Target velocity information, for simple scenarios (e.g. when imaging balloons, gliders, terrain, and other simple stationary objects), can be determined by applying a smoothing filter (low-pass or median) to the raw FFT data, and then executing a peak finding algorithm to determine the main target velocity. Equation (2) can then be used to obtain the target velocity in m/s. This procedure is illustrated in Fig. 6. The target utilized to generate the data in Fig. 6 was a human walking directly toward the RADAR antenna.

Further analysis reveals the importance of the smoothing filter and *a priori* knowledge of the expected types of signals. The target shown in Fig. 6 was swinging its arms while walking toward the antenna. Moreover, there were other additional sources of motion (e.g., clothing, and legs) whose motion was not completely parallel to the main lobe boresight vector. This results in target spectral broadening. Since other targets tend to have similar movement patterns, *a priori* knowledge is needed to determine the type of post-processing required to extract the desired information. For example, multiple targets traveling at similar velocities (relative to the RADAR antenna) would have their individual signatures merged into a single average velocity after the filtering operation.

5.2. Complex targets: Rotorcraft

Targets assumed to be "complex" are evaluated in a different manner. This is due to the presence of a relatively predictable signal structure that enables target identification. The nature of the signals can be seen in Fig. 7. This method of target identification starkly contrasts with other methods applied to larger vehicles such as high-resolution range profiles.[11]

Figure 7 displays the instantaneous Doppler frequencies of three miniature vehicles: a coaxial rotor helicopter (E-Sky Lama v4), a commercially available quadrotor (Parrot AR Drone,[12] see Fig. 4), and the TREX 450 Pro. When compared against the RADAR signature of a human, the rotorcraft exhibit a less complex signature.

An examination of Fig. 7 shows that most of the signal energy is present in the lower frequencies. While the signals generated by the downconversion process bear higher frequency components, these higher frequencies are filtered by the IF amplifier module leaving their lower frequency harmonics.

This characteristic of the prototype RADAR system is advantageous in that one can use it to determine the velocity of the target relative to the sensor. This is done by reducing the number of samples that comprise a signature from 256, and sliding this truncated target signature along the 256-sample scene signature, determining the match quality at each point. If the best match occurs at a non-zero offset, then the target bears a radial velocity corresponding to the offset.

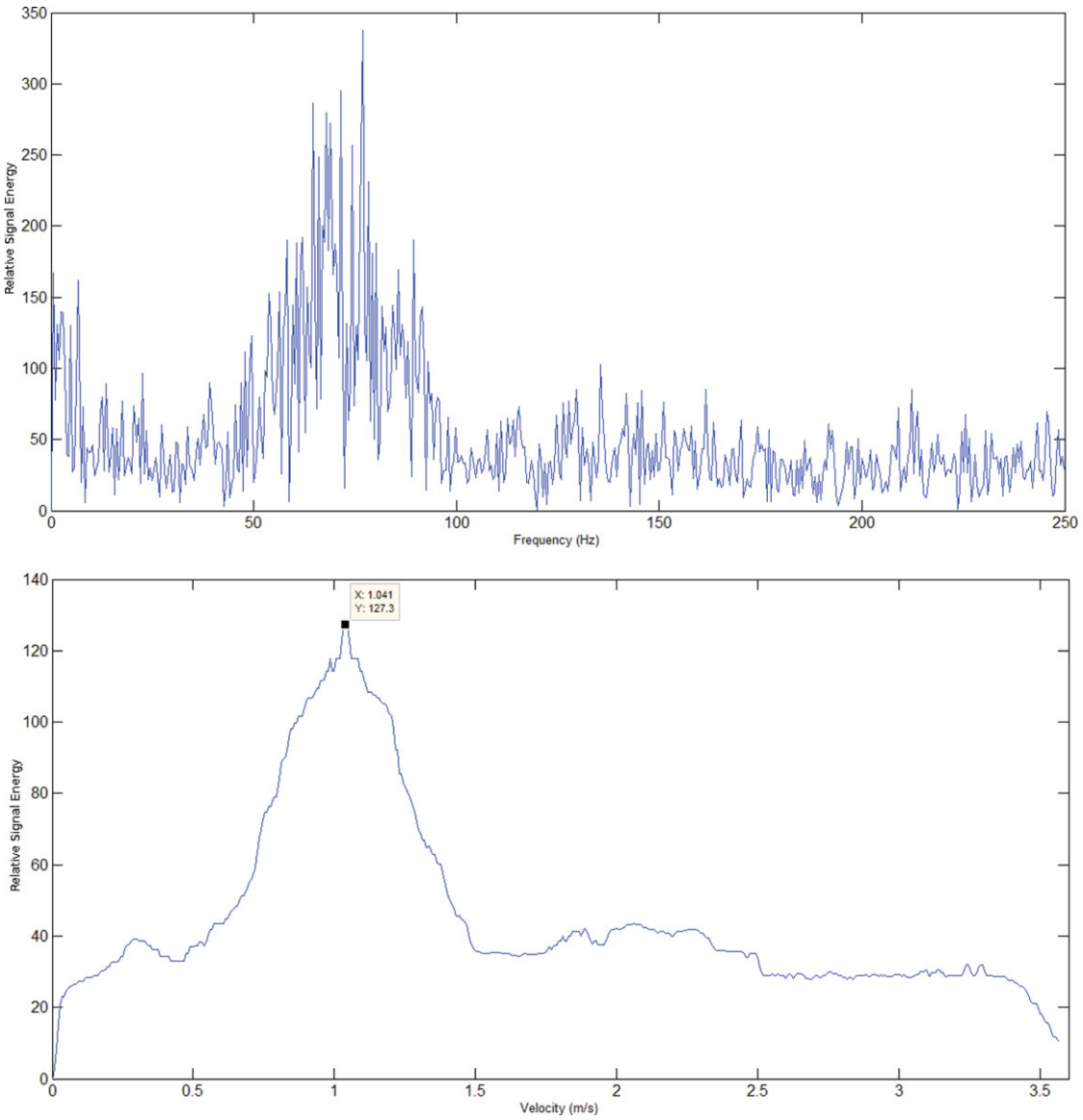

Fig. 6. (Colour online) Point target: walking human.

5.3. Target library

As described earlier, advanced control strategies for unmanned UAVs require both detection and identification. In order to detect the presence of a target of interest, one must differentiate a given signature from the background scene within the range of the sensor. In order to identify different targets, one must determine that a given signature matches one of a database of pre-recorded signatures of vehicle classes of interest. Fundamentally, both of these operations involve comparing a given "live" signature with a library of pre-recorded signatures and determining which is the best match. Both the background and vehicle signatures are represented within this signature library, and we are able to perform detection and identification in the same computational step (i.e., if the live signature matches the background signature the best, then we know there is no target of interest within range).

6. Target Identification Evaluation

A simple user interface to the RADAR system is implemented over a bi-directional serial link that enables it to operate in either data collection mode or target matching mode. Two different evaluation analyses are performed. In the first, the data collection mode is used to gather a large number of

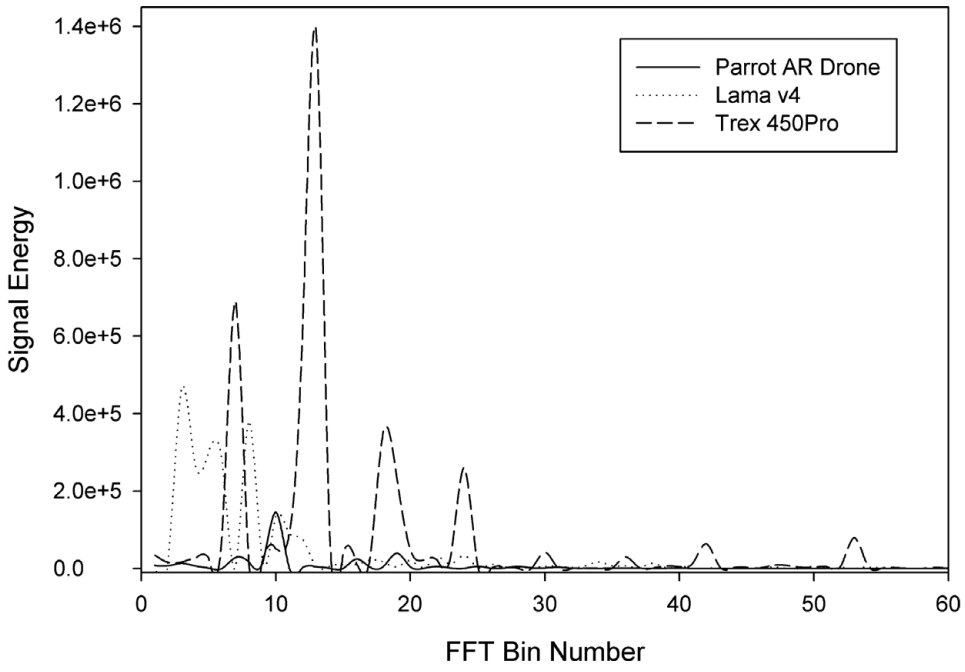

Fig. 7. Miniature rotorcraft signatures.

live samples of different vehicles in order to evaluate different matching algorithms off-line. The second evaluation performed is aimed at determining whether the RADAR system can successfully implement the matching logic on-board in a real-time scenario with live targets.

6.1. Matching algorithms

As previously described, the fundamental computational operation performed by the RADAR system is to match an incoming "live" signature against a library of pre-recorded vehicle signatures. In order to evaluate different algorithms efficiently, the data collection mode of the sensor was utilized to record 160, 256-sample signatures for the three vehicles whose signatures are depicted in Fig. 7.

For these experiments, the RADAR system and target vehicles are placed inside a reinforced concrete room. Throughout the experiments, the range between the RADAR system and target vehicles is fixed at 3 m (10 feet). The linear separation distance between each vehicle was 0.6 m, resulting in an angular separation of 11.31°. No effort was made to reduce or account for multi-path signals or reflections from the background. The vehicle signatures are recorded by fixing the vehicle to the floor of the test room and throttling the rotor system to typical flight speeds. The RADAR system is then pointed at the target vehicle and a series of signatures are streamed back to the attendant PC over the dedicated (wired) serial link; 160 of these signatures are gathered per vehicle and saved into a log file.

Due to the presence of noise in the signatures, experimentation with averaging a varying number of raw signatures into a "library signature" was done using a simple arithmetic average per sample position. For example, when averaging 10 signatures, all 10 values in the first of 256 buckets are combined to give the average value for the first bucket. For each such library signature, a comparison was made between it and all other signatures by averaging the same number of raw signals across the three vehicles. Identification was performed by calculating the best match across all vehicles using the algorithms described below. If the best match comes from the correct vehicle, it is counted as a successful match.

Each algorithm computes a single match value when executed on a library signature and live signature pair. The vehicle corresponding to the library signature that exhibits the best match with the live signature is selected. The following simple algorithms were evaluated due to their rapid execution time on embedded hardware.

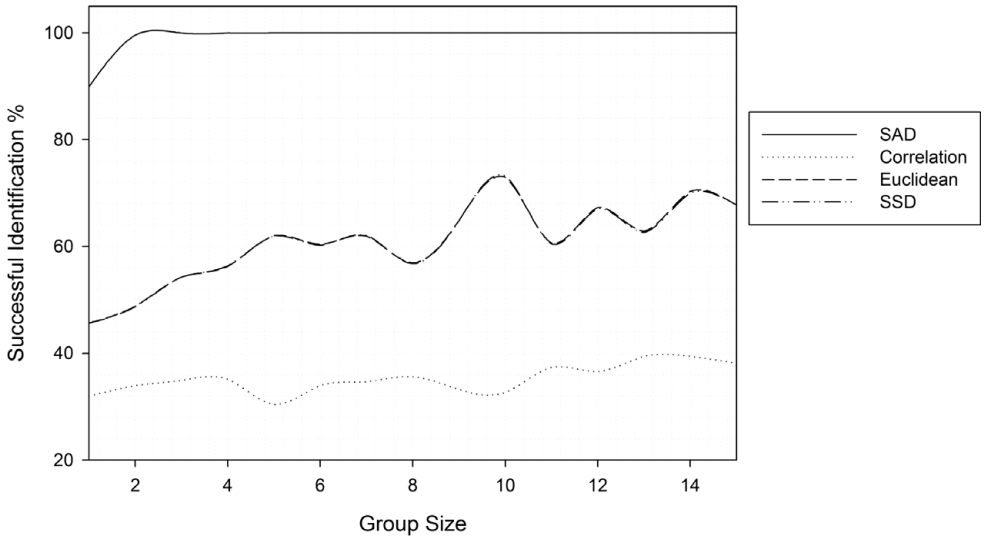

Fig. 8. Comparison of algorithm effectiveness versus the number of signatures averaged.

- *Sum of absolute differences (SAD)*. The total difference between the two signatures is calculated by adding the absolute value of differences between the 256 samples. The match with the smallest total difference is taken as best.
- *Sum of squared differences (SSD)*. The total difference between the two signatures is calculated by adding the square of differences between the 256 samples. The match with the smallest total difference is taken as best.
- *Euclidean distance (ED)*. The total distance between the two signatures is calculated by taking the square root of the sum of squared differences. The match with the smallest total difference is taken as best.
- *Correlation (C)*. The correlation between the two signatures is calculated by taking the average pairwise product of the 256 samples. The match with the maximum correlation is taken as the best.

The results of this evaluation are depicted in Fig. 8. The vertical axis contains the percentage of correct matches, while the horizontal axis represents the varying number of raw signatures being averaged. The averaging of signatures in these algorithms represents a tradeoff between accuracy and speed. In all algorithms evaluated, averaging more signatures improves the accuracy. However, with larger group sizes the time needed to acquire and process the signals dramatically reduces the effectiveness of the RADAR for collision avoidance.

The algorithm with the best performance is clearly the SAD algorithm that exhibits almost perfect accuracy when at least three signatures are averaged. The SSD and ED algorithms exhibit moderate performance, and the correlation algorithm performs poorly. This is significant for two reasons: (i) SAD is a simple and fast algorithm to execute on a microprocessor requiring only a handful of arithmetic operations for each sample, and (ii) only having to average a small number of raw signatures to successfully differentiate vehicle classes means our sensor can be utilized in a real-time scenario to perform the advanced control operations desired.

6.2. Live target identification

Utilizing the same basic setup as described above, the ability of the RADAR system to differentiate between live targets with the matching algorithm implemented on the XMOS microcontroller was evaluated.

The test procedure begins with recording the background Doppler signature, which is then subtracted from subsequent measurements.

The library signature for each vehicle is recorded by averaging 30 raw signatures. It is this average signature that is used to identify the vehicle in subsequent measurements. This procedure was repeated for all three vehicles. Once the signatures for all the vehicles have been acquired, target identification can begin. Note that in a deployed RADAR system, however, these signatures are likely to be stored

in non-volatile memory on-board the sensor processor or transmitted to the sensor by the UAV's mission computer as needed.

The initial round of live target testing simulated a single target scenario (although the other targets were present, the rotors on the other vehicles were not moving). The RADAR system was pointed at each target, in turn, and the rotors on the respective target were brought to typical flight speeds. As anticipated by the earlier tests, the results with the SAD algorithm resulted in approximately 100% correct identification.

The second round of live target testing simulated multiple UAVs sharing the airspace in the region ahead of the host UAV. Two UAVs, in this case the Lama v4 and the TRex, were operated and the RADAR sensor was pointed at each vehicle in turn and a match was computed. Despite the difference in vehicle size, the RADAR system correctly identified the target directly in front of the sensor despite the "noise" generated by the other vehicle.

6.3. Flight mounted on the parrot

Finally, to demonstrate the claim that the RADAR system can be mounted on miniature UAVs, the sensor was mounted onto a Parrot AR Drone. The prototype sensor is 230 g; the Parrot AR Drone, without the protective fairing, is able to hover with the sensor on-board. It should be noted that the vehicle was operated 1600 m above sea level. Furthermore, the Parrot AR Drone is not designed to carry a payload; therefore, by all metrics (e.g. flight time, wind resistance, and forward velocity) the vehicle's performance was reduced. However, the tests were successful when considering the limitations of the host vehicle.

6.4. Linear discriminant analysis

Although the algorithms that were applied in real time have shown very promising results, it is essential to further examine the nature of the sensed data. To that end, a series of data collection experiments were set up, in which the target aircraft is placed at a known distance and at a series of known angles with respect to the axis of the main lobe of the sensor. The vehicles chosen are a coaxial miniature helicopter and a quadrotor. The vehicles are placed in a 0°, 90°, 180°, and 270° angles with respect to the RADAR system. The samples corresponding to the coaxial helicopter were taken with the motors at half and full speed. While care was taken to acquire an equal number of samples for each configuration, due to noise, some of the samples were corrupt. This resulted in a data set of 1439 samples of 256-dimensional FFT vectors. Using linear discriminant analysis (LDA), it is possible to distinguish between the two types of targets with excellent consistency. The method searches for a linear hyperplane in the 256-dimensional space that will separate the samples belonging to the two different classes, in this case the coaxial and the quadrotor vehicles. Every sample x_i for which $x_i \cdot A + B > 0$, where A is the 256-dimensional vector and B is the scalar that defines the discriminant hyperplane and a threshold, respectively, is classified as belonging to class "coaxial." Otherwise, it belongs to class "quadrotor." The values for A and B are calculated by the LDA.[13] The function $x_i \cdot A + B$ acts as a projection function from the original 256-dimensional space to a single-dimensional space.

An example of this classification is shown in Fig. 9, where the samples of the data set have been projected to either side of zero. That particular example included some heavily corrupted measurements which appear as a small cluster in the "quadrotor" region. To evaluate the LDA approach, 80% of the data set was selected as training data and evaluated against the remaining 20%. Repeating the process for 1000 iterations yielded average correct classification rates of 99.99% and 99.23% for the samples belonging to the "coaxial" and "quadrotor" classes, respectively. Table II shows the confusion matrix that also includes the misclassification rates. For example, out of the actual samples corresponding to the "coaxial" class the classifier classified 99.997% as "coaxial" and 0.003% as "quadrotor." The correct classification rates for each of the 1000 iterations are shown in Fig. 10.

Future research will focus on exploring the possibility of inferring, not just the type of the target, but its orientation as well. Subsequent work will also include the reduction of the dimensionality of the feature vector that will reduce the, already relatively low, computational cost of the classification process.

Table II. Confusion matrix for the two-class problem.

		Predicted	
		Coaxial	Quadrotor
Actual	Coaxial	99.997%	0.003%
	Quadrotor	0.772%	99.228%

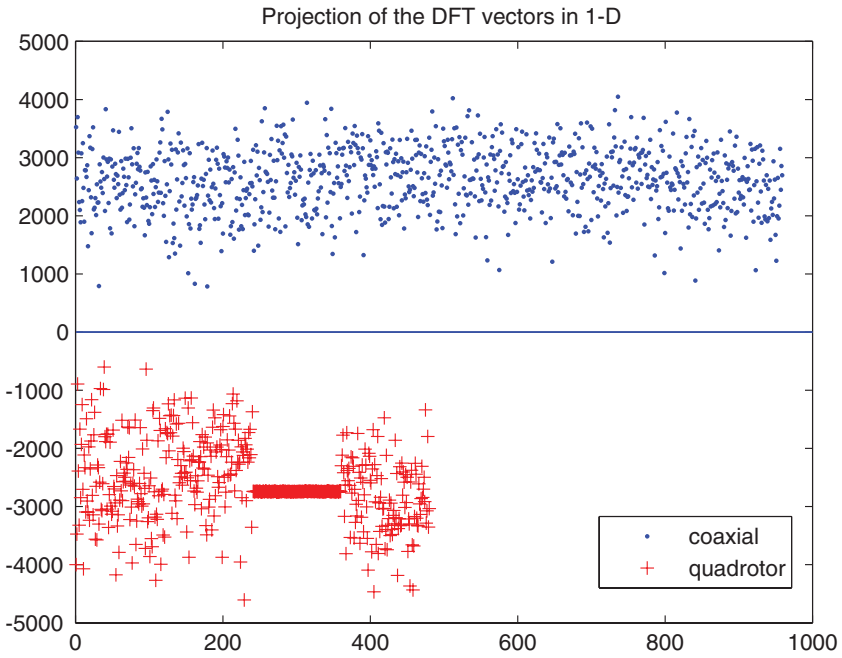

Fig. 9. (Colour online) Projection of the samples in the 1D subspace.

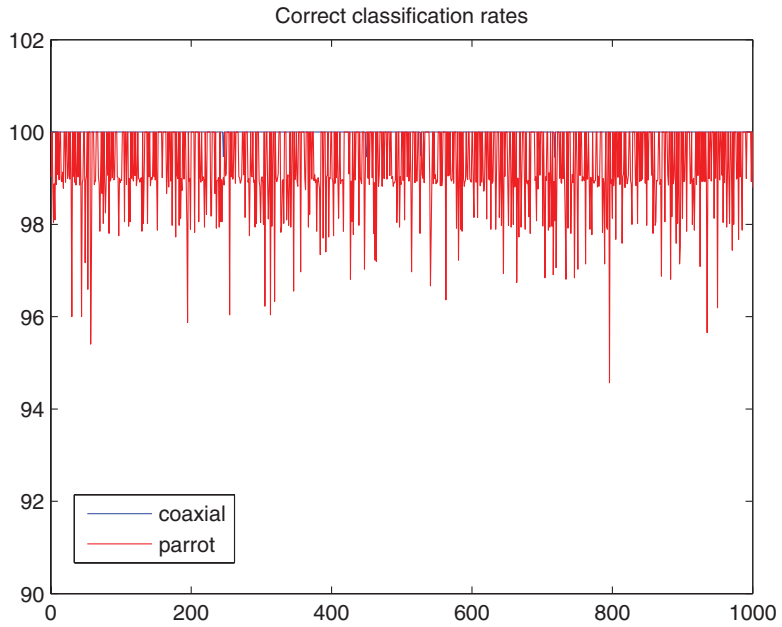

Fig. 10. (Colour online) Correct classification rate over 1000 iterations.

6.5. Outdoor tests

While the initial indoor tests, first reported in ref. [1] had a positive outcome, by virtue of being the first experiments, they had a number of shortcomings, namely:

- *Indoor environment*. All experiments were conducted in a target-poor environment (aside from the subject vehicle) at off hours to reduce interference from outside effects.
- *Co-planar RADAR and target arrangement*. The RADAR system was intentionally mounted on the floor with a clear field of view to the target vehicles. The antenna was positioned in front of the operators and computer equipment used to conduct the experiments. Additionally, the antenna was aimed at a portion of the building that was underground, and so not likely to have spurious background signals.

Therefore, it is necessary to evaluate the performance of the sensor while mounted on a rotorcraft at flight in an outdoor setting. This evaluation is critical to verifying the practicality of the sensor, both from a weight and flight dynamics perspectives as well as to determine if the RADAR would function well in a more realistic scenario.

There were initial concerns regarding the signal-to-noise ratio when installed on a rotorcraft or other aircraft. In other words, there exists a possibility that the energy of the signal reflected from the intended target would be small compared with the signal reflected from the host vehicle's propulsion system. In essence, there is a chance that the distant signal would be drowned out by the close signal making detection difficult.

Throughout the outdoor test sequence, this situation was not encountered; the signal from the host vehicle (i.e., without any other vehicles operating within the field of view of the sensor) was negligible and easily accounted for.

Additional concerns include the resilience of the sensor to a dynamic background. During initial feasibility experiments, the background was assumed to be static. However, in a more realistic setting, the background cannot be assumed to be a static phenomenon as the host vehicle will most likely be engaged in translational flight at some point during the mission. Fortunately, the frequency shift generated by the host vehicle's movement is relatively easily estimated by means of a satellite navigation system. The entire received spectrum can be frequency shifted using the microprocessor to provide corrected velocity measurements. In other words, since the host vehicle's velocity is known, it is relatively easy to integrate this information into the sensor's signal processing logic.

More importantly, however, there exists the possibility of motion caused not by the host or target vehicles, but by environmental factors. This includes the swaying of grass, trees, and the activity of wildlife in general. In all cases, these undesired signal returns can be classified as noise. It should be noted, however, that the Doppler frequency (and therefore the velocity) of most noise sources is low compared with the propulsion systems utilized in most aircraft, e.g. rotor blades, propellers, and jet engine compressors. Moreover, as shown in previous tests, each vehicle model has a unique Doppler signature that is unlikely to be duplicated by a randomly moving background.

These concerns are addressed by placing the RADAR system on a quadrotor UAV (Fig. 11) and attempting to detect and identify a conventional-type miniature helicopter (Fig. 12) in an outdoor environment. Throughout the test, the distance between the vehicles was approximately 7 m. The first procedure is the acquisition of a background radiation sample. This sample consists of the average frequency spectra over a short period of time and represents an environment absent of all targets of interest. Due to the need to compensate for the host vehicle's propulsion system, the quadrotor's propellers were operating slightly below take-off speed throughout acquisition. The target vehicle signature was recorded by aligning the target vehicle with the radar antenna boresight and recording the target signature with both vehicles rotor systems active, but still on the ground.

The sensor evaluation procedure consists of alternately inserting and then removing the target vehicle from the main lobe of the antenna. Throughout the process, the output of the target identification algorithm is continuously monitored to verify the correlation between the target identity and the actual presence of the vehicle. The results of this test series are similar to the tests performed in a controlled environment: the target vehicle was detected and correctly identified with accuracy approaching 100%. It should be noted that this stage of tests required both vehicles to remain on the surface, but with rotors active.

The final round of tests involved the use of the RADAR system with both vehicles airborne. The results of these final tests suffered a significant decrease in accuracy due to the difficulties involved

Fig. 11. (Colour online) Quadrotor equipped with the RADAR sensor.

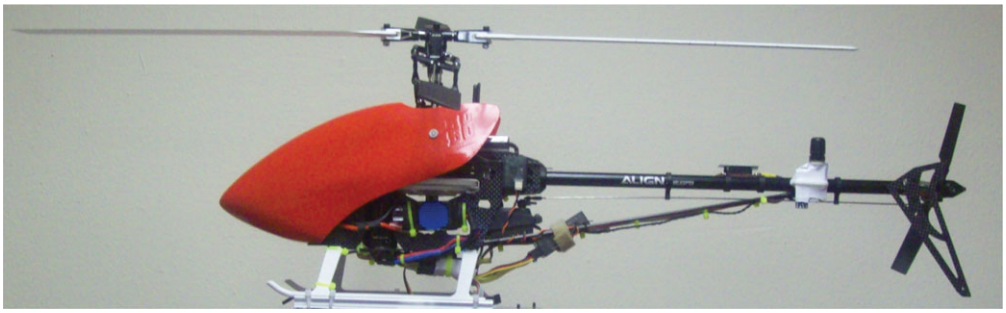

Fig. 12. (Colour online) Target vehicle.

in maintaining the target vehicle within the radar main lobe (approximately 12.5° off boresight). However, it is believed this is not a problem with the RADAR *per se*, but rather with the practical difficulty of maintaining two aerial vehicles at similar altitudes, and in an arrangement such that the target vehicle is within the main lobe of the RADAR in an outdoor setting. In some ways, the difficulty of performing flying experiments backs up the main claim that the RADAR is sensitive to other similar-sized vehicles operating in direct flight path—if the RADAR's main lobe was not relatively focused, it would be much easier to conduct this experiment.

7. Collision Avoidance Discussion

Detection range. As the goal of the RADAR system is to enable autonomous aircraft to avoid collisions with other air traffic, it must be shown that the RADAR system is capable of providing enough warning to allow the unmanned vehicle system to successfully evade airborne threats. This evaluation is performed by analyzing the ability of the host vehicle to determine the acceleration characteristics and then comparing the vehicle performance with the dimensions and typical velocities of potential threats. If the identity of the opposing aircraft is not available, the algorithm proceeds utilizing the worst-case scenario. This essentially means performing the evasion calculations using the opposing aircraft model that requires the largest clearance space and travels with the highest velocity. The host vehicle used for the outdoor tests (see Fig. 11), and has a maximum thrust of 3 kg at sea level. This results in a maximum vertical acceleration of 2 m/s^2, ignoring the effects of air resistance. Table III displays a number of aircraft, their typical speeds, and the time required to perform an altitude change significant enough to mitigate a midair collision. An examination of these data and the RADAR

Table III. Collision avoidance maneuver time estimates.[16–19]

Aircraft	Typical velocity	Vehicle height	Evasion time required
DG-808 Sailplane	32 m/s	1.43 m	0.382 s
Cessna 172R	63 m/s	2.72 m	0.527 s
Learjet 40XR	239 m/s	4.31 m	0.663 s
Boeing 747	248 m/s	19.1 m	1.397 s

Fig. 13. (Colour online) Operating phases.

system processing speed results in a lower estimate for the requisite target detection range. This is illustrated in Fig. 13.

Operating phases. Figure 13 shows a radar-equipped UAV to the left. Adjacent to this UAV is a region whose width is defined as the time required to perform a collision avoidance maneuver multiplied by the closing velocity between the two vehicles. As the velocity of many small UAVs is relatively small compared with the cruising velocities of passenger planes, the width of this region is, in effect, the worst-case scenario for this paper, and is determined by multiplying columns 2 and 4 of Table III and selecting the largest value. This represents the hardest target to evade. The next region, the detection region, is defined as the distance decrease between the two vehicles during the time taken by the sensor to detect and identify the target. This time is, in turn, affected primarily by the signal processing hardware and the algorithms utilized. Finally, the last region, the safety region, is essentially some multiple of the combined detection and evasion region distances. An example of this structure is as follows. If the sensor with a 2-Hz update rate is to avoid a Boeing 747 traveling at cruise velocity, the sum of the detection and avoidance regions is 471 m. Finally, for a factor of safety of three, the total region size width becomes 1413 m. It should be noted that this analysis makes no effort to determine the precise maneuver required to avoid a collision, and indeed this topic is outside the scope of this paper.

Effect of collision. In the event that a collision does occur, the damage incurred by both aircraft could be fatal. The collision between a miniature UAV and manned aircraft can be approximated by noting the similarities between the many small unmanned air vehicles and birds. This is useful as the damage caused by birdstrikes is well studied. Birdstrikes cause more than 1.21 billion USD worth of damage each year and the destruction of no less than 52 aircraft in general aviation alone.[14] This level of damage is understandable considering the energies involved. To estimate the energy transferred to the airframe, consider the kinetic energy of the bird relative to the airplane (see Eq. (5)). For example, a Learjet 40XR intercepting a 2-kg UAV at cruising velocity would result in an energy transfer of approximately 57 kJ. This is contrasted with the approximately 54 kJ delivered by the impact of a 20-mm anti-aircraft cannon.[15]

$$E = \frac{1}{2}mv^2. \tag{5}$$

8. Conclusion

As unmanned, autonomous aerial vehicles become more common for non-military applications, lightweight, low-energy, and precise mechanisms will be needed to allow the vehicles to operate safely in proximity to regular manned vehicles. We believe that both detection and identification will be critical to performing this function since unmanned vehicles may be expected to stay out of the flight paths of manned vehicles. In this paper, we present an overview of the design of a prototype miniature RADAR system, its evaluation in a realistic, outdoor environment, and an analysis of the capabilities required to enable UAV integration into the NAS. A major component of the work involves the use of micro-Doppler modulation for the reliable identification of miniature aircraft. This

aircraft identification method can be scaled to facilitate its application to larger vehicles. This is due to similar features being present on both large scale and miniature aircraft. The identification of larger aircraft is also facilitated by the presence of more distinctive features such as gas turbine engines and the comparatively large RADAR cross section (RCS) of the propulsion components. Finally, the micro-Doppler modulation method of identification is better suited to a wider range of aircraft sizes than the competing method: high-resolution range profiles.[11] This is due to the size of many UAVs being smaller than the range resolution of many pulsed RADAR systems and therefore appearing as a single point (rather than the range profile required for alternate methods of identification).

References

1. A. Moses, M. J. Rutherford and K. P. Valavanis, "Radar-Based Detection and Identification for Miniature Air Vehicles," **In**: *IEEE Conference on Control Applications*, Denver, CO. (2011).
2. A. Moses, M. J. Rutherford, M. Kontitsis and K. P. Valavanis, "UAV-borne X-band Radar for MAV Collision Avoidance," **In**: *Proc. SPIE 8045, Unmanned Systems Technology XIII, 80450U* (May 23, 2011).
3. *Introduction to TCASII, Version 7*, U.S. Department of Transportation, Federal Aviation Administration (Nov. 2000).
4. ICAO, *ICAO Doc. 7030/4 (Region Supplementary Procedures)*, 5th ed. (International Civil Aviation Organization, 2008).
5. "TCAS/ACAS," Forecast International, Technical Report (January 2007).
6. Z. F. Systems, "PCAS MRX product page," Zaon Flight Systems, Technical Report.
7. "FLARM technical overview – how does it work ?" Gliderpilot.org, Technical Report.
8. "FLARM faq," Gliderpilot.org, Technical Report.
9. J. Volakis, "Horn Antennas," **In**: *Antenna Engineering Handbook*, 4th ed. (McGraw-Hill, New York, NY, 2007).
10. L. Technology, *LTC1864/LTC1865*, Linear Technology Corporation.
11. P. Tait, *Introduction to RADAR Target Recognition* (London, UK: Institute of Engineering and Technology, 2005).
12. P.-J. Bristeau, F. Callou, D. Vissière and N. Petit, *The Navigation and Control Technology Inside the AR.Drone Micro UAV* (IFAC World Congress, Milano Italy, 2011).
13. R. O. Duda, P. E. Hart and D. G. Stork, *Pattern Classification*, 2nd ed. (Wiley, Hoboken, NJ, 2001).
14. J. R. Allan and A. P. Orosz, "The Costs of Birdstrikes to Commercial Aviation." 2001 Bird Strike Committee-USA/Canada (2001).
15. S. V. Lieven Dewitte, "M61 a1 vulcan: 20 mm gatling gun system," Technical Report.
16. D. Flugzeugbau, "DG-808: The High-Performance Sailplane and Motor Glider," DG Flugzeugbau, Germany.
17. Cessna Aircraft Company, "Skyhawk model 172r: Specification and description" (May 2010).
18. Bombardier Aerospace, Business Aircraft, "Learjet 40xr factsheet."
19. Boeing Commercial Airplanes, "747-8 airplane characteristics for airport planning" (Sep. 2008).